



<http://www.diva-portal.org>

Postprint

This is the accepted version of a paper published in *Composites Science And Technology*. This paper has been peer-reviewed but does not include the final publisher proof-corrections or journal pagination.

Citation for the original published paper (version of record):

Gutkin, R., Costa, S., Olsson, R. (2016)

A physically based model for kink-band growth and longitudinal crushing of composites under 3D stress states accounting for friction

Composites Science And Technology, 135: 39-45

<https://doi.org/10.1016/j.compscitech.2016.09.002>

Access to the published version may require subscription.

N.B. When citing this work, cite the original published paper.

Permanent link to this version:

<http://urn.kb.se/resolve?urn=urn:nbn:se:ri:diva-40971>

A physically based model for kink-band growth and longitudinal crushing of composites under 3D stress states accounting for friction

Renaud Gutkin*, Sérgio Costa, Robin Olsson

Swerea SICOMP AB, SE-431 22, Mölndal, Sweden

ARTICLE INFO

Article history:

Received 23 December 2015

Received in revised form

2 August 2016

Accepted 1 September 2016

Available online 3 September 2016

Keywords:

Crushing

Fibre kinking

Friction

Damage mechanics

ABSTRACT

A material model to predict kink-band formation and growth under a 3D stress state is proposed. 3D kinking theory is used in combination with a physically based constitutive law of the material in the kink-band, accounting for friction on the microcracks of the damaged material. In contrast to existing models, the same constitutive formulation is used for fibre kinking and for the longitudinal shear and transverse responses, thereby simplifying the material identification process. The full collapse response as well as a crush stress can be predicted. The model is compared with an analytical model, a micro-mechanical finite element analysis and crushing tests. In all cases the present model predicts well the different stages of kink-band formation and crushing.

1. Introduction

Understanding, modelling and finally predicting the compressive response of continuous Carbon Fibre Reinforced Plastics (CFRP) materials is a long standing and unresolved issue. It is however an important one as kink-band formation is a failure mode responsible for high energy absorption in compression. Currently available meso-models use linear degradation of the stresses based on toughness values for kink band formation [1], which are hard to measure and very scattered. The present model eliminates the need for fibre kinking toughness measurement, and considers the energy absorbed by friction once the material has been fully damaged. Such an approach is important in areas where it is not only necessary to accurately predict the compressive strength (peak stress) but also the post-peak behaviour. For example, the model is interesting for simulation of crash structures in car applications, for predicting the response of bolted joints and for the residual response of composite structures subjected to impact.

Compressive failure of fibre composites may involve splitting failure, kinking failure or a combination of both [2]. Splitting failure often occurs at the fiber-matrix interface within the kink-band as shown in Ref. [3]. Because of the large strains involved, a significant amount of the stored energy can be released during splitting [4].

Thinner fibres and higher fibre volume fractions were shown to promote kinking failure [2]. The current paper is focused on structural carbon fibre composites, which typically fail in kinking for fibre volume fractions between 10 and 60%.

Improving from the first strength models based on kinking induced by microbuckling developed by Rosen [5], the matrix shear strength was later on accounted for by Argon [6] and Budiansky [7]. The resulting equation, Eq. (1), predicts the longitudinal compressive strength, X_c , under the assumption that kink-band formation occurs when the shear strength in the kink-band is reached due to further rotation of initially misaligned fibres

$$X_c = \frac{S_L}{\theta_i + \gamma_c} \quad (1)$$

where S_L is the in-plane shear strength, γ_c the shear strain at failure and θ_i is the initial fibre misalignment. Eq. (1) is a key equation in fibre kinking theory, a framework which has been extended to predict the collapse response [8]. The collapse, or post peak, response was predicted for 2D stress states and using a nonlinear elastic response (Ramberg-Osgood model) for the material in the kink-band [8] or Schapery theory in Ref. [9]. A typical response shows a strain softening after the peak load and a flattening of the curve at larger strains.

Similar collapse responses were predicted by analytical micro-mechanical models based on couple stress theory [10–12]. These models account for fibre bending and show that it can be neglected

* Corresponding author.

E-mail address: renaud.gutkin@gmail.com (R. Gutkin).

in predicting failure although it plays an essential role in the calculation of kink-band width. The effect of multiaxial 2D loading was later considered in Ref. [13], where it was shown how the axial compressive strength was increased by transverse compression, and reduced by transverse tension.

While some of the previous models have been implemented in a Finite element (FE) framework, they do not handle 3D stress states. Under such stress states, Pinho et al. [1,14] proposed a model based on fibre kinking but where failure initiation is predicted by a Mohr-Coulomb criterion.

In the present contribution, the 3D fibre kinking theory proposed in Ref. [1] is extended to also predict the collapse response. The post peak response follows the work by Refs. [8,9] but provides an improved response of the material in the kink-band compared to these models. To this end, the model uses a constitutive law based on progressive damage enhanced to account for contact and friction at microcrack closure under compressive loading [15]. The work presented here together with the model developed in Ref. [15] provides a unified and physical approach to model crushing both for compressive matrix failure and fibre kinking failure. In particular, the model proposes a physical solution to the different stages of energy dissipation, first during damage formation and second by friction during the crushing.

2. Formulation of the model

The objective of the model is to predict the longitudinal compressive response ($\sigma_{11} < 0$) for a transversely isotropic ply under an arbitrary loading. In the longitudinal direction, loading is strain driven due to the collapse nature of the response and the resulting strain softening. For direct and shear loading in the other directions both stress and strain can be prescribed.

Matrix damage introduced by in-plane shear and the transverse loading is accounted for by using the nonlinear constitutive law derived in Ref. [15]. This constitutive law is also used to describe the response of the material in the kink-band. In short, the fibre kinking response is found from solving (i) a stress equilibrium between applied global stresses and nonlinear local stresses resulting from (ii) the nonlinear constitutive law of the material in the kink-band. The actual rotation of the fibres in the kink-band, θ , is defined as a state variable and resolved from (iii) the strain compatibility. The three conditions (i) to (iii) must be solved simultaneously. This is described below after a description of the conventions.

2.1. Geometrical description and notations

Throughout the manuscript, the conventions and notations defined in Fig. 1 will be used.

Fig. 1(a) shows a micrograph of a kink-band formation with typical parameters, where w is the kink-band width and β is the kink-band angle. A unidirectional lamina under a general compressive stress state is shown in Fig. 1(b). Two coordinate systems are introduced. The first one corresponding to the orientation of the kink-band through the thickness is denoted r and is characterised by the angle ψ . The second (misaligned) coordinate system, m , is associated with the rotating fibres and is characterised by the angle θ , Fig. 1(c). Fig. 1(d) defines the initial and current configurations and associated fibre rotations. The numerical subscripts (11, 22, 12) refer to the global coordinate system and the subscripts using m (11 m , 22 m , 12 m) refer to the misaligned frame, m , also referred to as local frame later on.

2.2. Stress equilibrium

A kink-band forms when nonlinearities occur in the matrix

material between fibres rotating under a compressive load. To predict initiation and growth of kink-bands, the equilibrium equations between the applied external stresses and the local stresses need to be solved. In a 3D framework it is assumed that fibres will form planes of kinked fibres, Fig. 1(b), i.e. that no out of plane shear stresses are acting on a kink-band plane. This assumption was introduced in Ref. [1] and gives the following equation for the angle ψ :

$$\psi = \frac{1}{2} \tan^{-1} \left(\frac{2\tau_{23}}{\sigma_{22} - \sigma_{33}} \right) \quad (2)$$

Knowing ψ , the stress in the r coordinate system, σ_r , can be found from the global stress as follows:

$$\sigma_r = \mathbf{T}_\psi \sigma \mathbf{T}_\psi^T \quad (3)$$

where \mathbf{T}_ψ is the transformation matrix for the angle ψ and where $\mathbf{T}_\psi^T \mathbf{T}_\psi = \mathbf{I}$.

The local equilibrium to be solved is expressed in the m coordinate system as

$$\sigma_m - \mathbf{T}_\theta \sigma_r \mathbf{T}_\theta^T = 0 \quad (4)$$

Where \mathbf{T}_θ is the transformation matrix for the angle θ and where $\mathbf{T}_\theta^T \mathbf{T}_\theta = \mathbf{I}$ and σ_m are the local stresses which results from the local strains through the constitutive law defined in the next section $\sigma_m = \mathcal{L}(\epsilon_m)$.

In the (1 m , 2 m) plane there are only three non-trivial equations

$$\sigma_{11m} - (\sigma_{11r}c^2 + \sigma_{22r}s^2 + 2\tau_{12r}sc) = 0 \quad (5)$$

$$\sigma_{22m} - (\sigma_{11r}s^2 + \sigma_{22r}c^2 - 2\tau_{12r}sc) = 0 \quad (6)$$

$$\tau_{12m} - (-\sigma_{11r}sc + \sigma_{22r}sc + \tau_{12r}(c^2 - s^2)) = 0 \quad (7)$$

where $c = \cos(\theta)$ and $s = \sin(\theta)$. The relation between fibre rotation and the in-plane shear in the misaligned frame is established from Fig. 1(d) as

$$\theta = \gamma_{12m} + \theta_i \quad (8)$$

2.3. Longitudinal shear and transverse responses

From Eq. (5)–(7), it can be seen that the longitudinal response derives from the response in the local coordinate system (m). In particular, the longitudinal (in-plane) shear τ_{12m} typically shows a significant nonlinear response, which results eventually in the collapse response in longitudinal compression due to a shear instability [1]. To predict the response and stresses in the kink-band, the constitutive law derived in Ref. [15] is used and is noted $\sigma_m = \mathcal{L}(\epsilon_m)$. For a given strain state $\epsilon = (\epsilon_{11} \ \epsilon_{22} \ \epsilon_{33} \ \gamma_{12} \ \gamma_{13} \ \gamma_{23})^T$, the constitutive law provides the stress state $\sigma = (\tilde{\sigma}_{11} \ \sigma_{22} \ \sigma_{33} \ \tau_{12} \ \tau_{13} \ \tau_{23})^T$, where the longitudinal component is calculated linear elastically, noted with $\tilde{\cdot}$. The other components are obtained from a fixed crack model in which the relation between the stresses and strains is obtained from the response in the plane determined at failure initiation and fixed during damage evolution. In this fracture plane, a new set of coordinates (NLT) is defined: normal, longitudinal and transverse to the fibres direction, see Fig. 2. The fixed crack formulation makes it possible to account for physical mechanisms

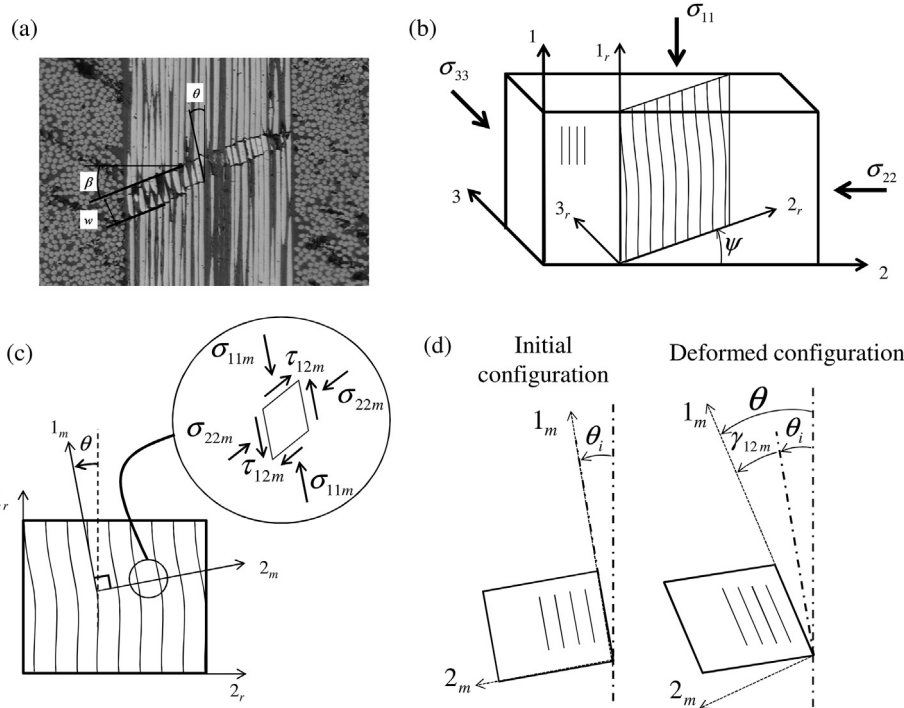


Fig. 1. Illustration of a 3D kinking model, adapted from Ref. [1].

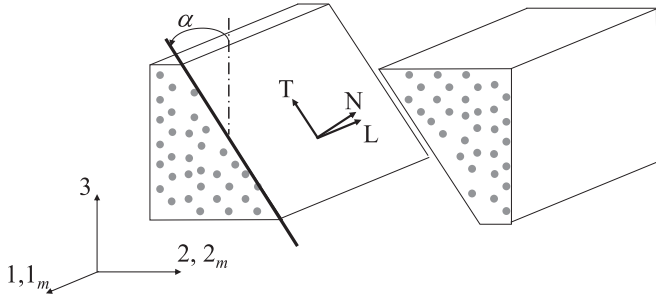


Fig. 2. Definition of the coordinate system for the fixed crack model.

on the fracture plane and in particular to couple damage growth with the friction generated during sliding of the fracture plane. The details of the derivations for the fixed crack models are given in Ref. [15] and only the main equations are summarised here.

The derivation of the coupling between the damage growth and the friction on closing microcracks is summarised in Eq. (9), where σ^{NLT} is the traction vector on the fracture plane, d is the damage variable, $\tilde{\sigma}^{\text{NLT}}$ is the undamaged traction vector and σ^{friction} is the vector associated with friction on the faces of the microcracks. Two state variables are introduced to describe the dissipation mechanisms, the damage variable, d , and a sliding strain, γ_s .

$$\sigma^{\text{NLT}} = \begin{cases} (1-d)\tilde{\sigma}^{\text{NLT}} + d \cdot \sigma^{\text{friction}} = \begin{pmatrix} \tilde{\sigma}_N \\ (1-d)\tilde{\tau}_L \\ (1-d)\tilde{\tau}_T \end{pmatrix} + \begin{pmatrix} 0 \\ d \cdot \tau_L^{\text{friction}} \\ d \cdot \tau_T^{\text{friction}} \end{pmatrix} & \text{for } \tilde{\sigma}_N < 0 \\ (1-d)\tilde{\sigma}^{\text{NLT}} & \text{for } \tilde{\sigma}_N \geq 0 \end{cases} \quad (9)$$

The friction component is defined using a Coulomb friction model with

$$\tau_i^{\text{friction}} = \begin{cases} G_i(\gamma_i - \gamma_s) & \text{if no sliding} \\ \mu_i \langle \tilde{\sigma}_N \rangle_- & \text{if sliding} \end{cases} \quad \text{and with } i = \{L, T\} \quad (10)$$

The evolution of the damage variable is governed by two equations, Eq. (11) which predicts the initiation of damage and Eq. (12) which gives the actual evolution with strain

$$f(t) = \max_{\substack{t' \leq t \\ \alpha \in [0, \pi]}} \left\{ \left(\frac{\tilde{\tau}_L}{S_L} \right)^2 + \left(\frac{\tilde{\tau}_T}{S_T} \right)^2 + \left(\frac{\langle \tilde{\sigma}_N \rangle_+}{Y_T} \right)^2 \right\} \quad (11)$$

$$d = \frac{\gamma^p - \gamma_0^p}{\gamma_f^p - \gamma_0^p} \quad (12)$$

where, S_L , S_T and Y_T are shear and tensile strengths, γ is the driving strain defined in Ref. [15] and γ_0 and γ_f are the strain at initiation and at full decohesion, respectively. The exponent p is a shape parameter similar to the one introduced in Ref. [16]. The damage variable is associated with matrix failure (i.e. with the longitudinal shear and transverse behaviour) but is also used for fibre kinking. In other words, fibre kinking is treated as a matrix failure mode, which implies that the evolution of a single damage is required, therefore removing the need to measure translaminar compressive, or fibre

kinking, toughness values.

2.4. Strain compatibility

The angle of the fibres in the kink-band θ is the second unknown and is found from the compatibility between global and local strains. The strains ε_r and ε_m in the local coordinates can be obtained in a similar fashion to the stresses in Eqs. (3) and (4) using the following transformations

$$\varepsilon_r = \mathbf{T}_\psi \varepsilon \mathbf{T}_\psi^T \quad (13)$$

and

$$\varepsilon_m = \mathbf{T}_\theta \varepsilon_r \mathbf{T}_\theta^T \quad (14)$$

Similarly to Eqs (5)–(7), Eq. (14) gives three equations in the $(1_m, 2_m)$ plane and the one for the shear component is used to solve for θ

$$\gamma_{12m} = \theta - \theta_i = 2(\varepsilon_{22r} - \varepsilon_{11r})s c + \gamma_{12r}(c^2 - s^2) = 0 \quad (15)$$

2.5. Numerical integration

To solve the nonlinear set of equations, the procedure shown in Fig. 3 is used. First, the applied stresses and strains are received as inputs and are used to evaluate matrix damage induced by longitudinal shear and transverse stresses. The constitutive law described in Section 2.3 is used and the longitudinal stress is calculated as linear elastic $\bar{\sigma}_{11}$. In particular, the two state variables: the damage variable and the sliding strain, are calculated and stored to be propagated to the next step. Subsequently, Eq. (4) and (15) are solved simultaneously for the couple of unknowns (σ_{11}, θ) . In this process, the stresses σ_m are calculated using the constitutive law described in Section 2.3 again and with the strain ε_m as input. The damage variable calculated in that step is called *dkink*, and corresponds to *d* evaluated in the *m* coordinate system. For a general 3D stress state, a convergence criterion so that $dkink \approx d$ should be fulfilled. These iterations are not performed for the examples shown here as only pure compressive loading is considered.

The model is implemented in the open source software Scilab and Eq. (4) and (15) are solved using Powell's method [17]. This method requires an initial guess for both unknowns. Because of the strain softening exhibited by the response, two initial guesses are given for the load increment, one positive load increment and one negative. A solution exists only in one of the two cases. The load

increments are constant throughout an analysis and the strain increments are kept small to guarantee that enough accuracy is achieved close to the peak load.

3. Identification of model parameters

The material parameters needed for the model are all extracted from standard tests. The material used in this paper is a carbon epoxy (HTS45/LY556) NCF composite material with an uni-weave architecture. This material was fully characterised and the data are reported in Ref. [18] and summarised in Table 1. The actual material is slightly orthotropic, but the current model assumes transverse isotropy, and hence matrix dominated properties are defined as the average of the measured properties in the 1–3 and 2–3 planes.

The exponent p used in the evolution of damage and the friction properties with index L are found from the longitudinal cyclic shear test shown in Fig. 4. The internal pressure p_{0T} is found from the transverse compression test and μ_T is assumed equal to μ_L . A description on the identification of these parameters is given in Ref. [15].

A comparison between the predicted in-plane shear response and cyclic experiments is shown in Fig. 4. It can be seen that the model captures well both the nonlinear behaviour and the hysteresis loops even though a discrepancy is seen as the strain becomes large. A perfectly plastic response used for comparison with an analytical model and a micromechanical FE model in the next section is also shown.

Table 1
Mechanical properties of the uni-weave NCF composite HTS45/LY556.

Elastic properties				
Modulus		Poisson's ratios		
E_{11} (MPa)	E_{22} (MPa)	G_{12} (MPa)	ν_{12} ()	ν_{23} ()
136000	9150	4900	0.29	0.4
Strength properties				
X_t (MPa)	Y_t (MPa)	S_L (MPa)	p	
1787	29	20	-0.7	
X_c (MPa)	Y_c (MPa)	S_T (MPa)		
626	130	47.44		
Friction properties				
Internal pressure		Coefficient of friction		
p_{0L} (MPa)	p_{0T} (MPa)	μ_L ()	μ_T ()	
60	30	0.4	0.4	

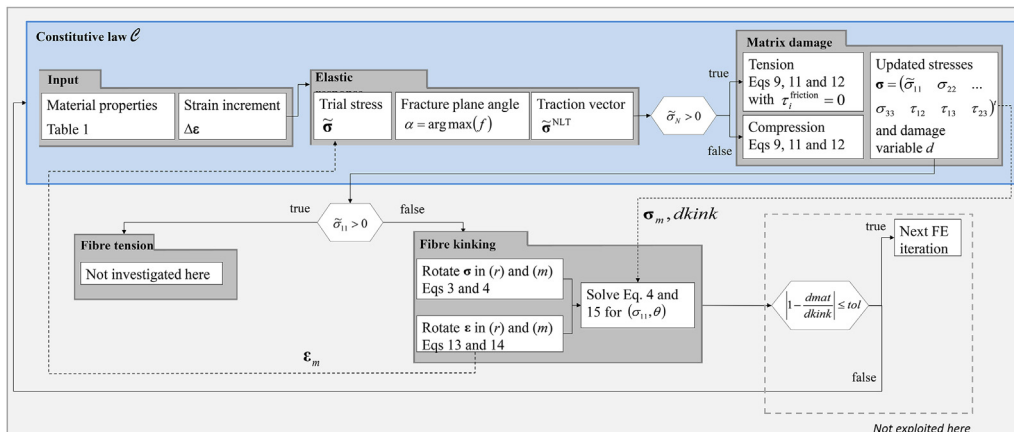


Fig. 3. Solution procedure for the present model. The dashed arrows (—) indicates the calculation of the local stresses σ_m .

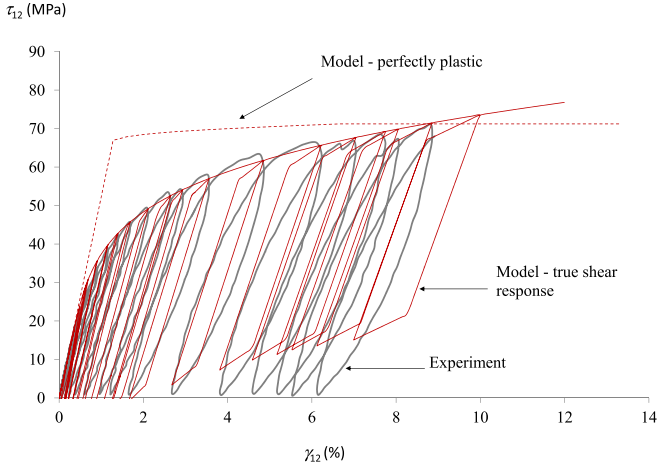


Fig. 4. Shear response for the HTS45/LY556 system – Experimental results versus model.

4. Results

4.1. Comparison with analytical and micromechanical FE models

The model is first validated against existing analytical and micromechanical FE models developed in Refs. [11,19]. Both models were validated for the carbon-epoxy system IM7/8552 and are here adapted to the HTS45/LY556 used in this study, with the assumed perfectly plastic response shown in Fig. 4. The models in their initial states are shown in Fig. 5, with the load applied in the x -direction.

Readers interested in the analytical and micromechanical FE models are referred to [11,19]. It is sufficient here to say that the analytical model is based on the equilibrium of an imperfect fibre, Fig. 5(a), laterally supported by an elasto-plastic matrix. The model is able to predict the initiation of yielding, identified as kink-band formation, as well as the post yielding and post peak response. A typical stress strain curve from this model is shown in Fig. 6.

The micromechanical FE model is based on a 2D representation of 100 fibres with a fibre diameter of 7 μm and intermediate resin layers of 1.6 μm . The fibres and matrix layers are also initially imperfect with a sinusoidal form, see Fig. 5(b). The model is run with an implicit, displacement controlled, analysis in the FE package Abaqus.

Fig. 6 shows a typical stress strain curve for the analytical, the micromechanical FE and the present models. All models are run

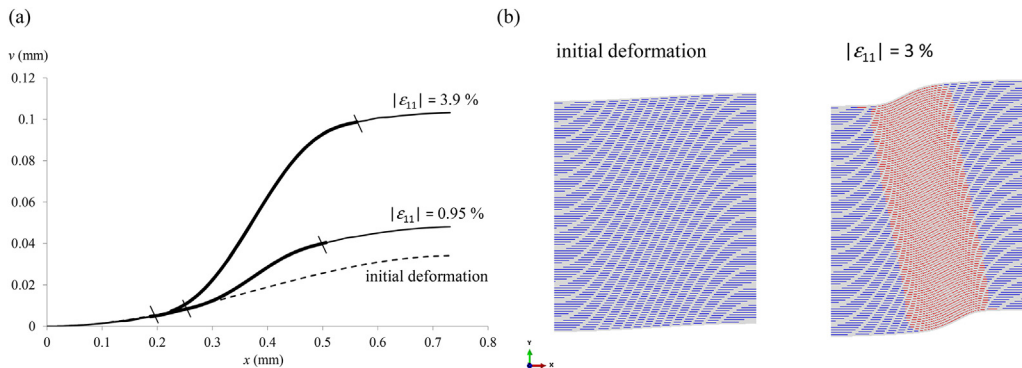


Fig. 5. (a) Deformation of the analytical model from the initial configuration to an applied strain of 3.9%. Matrix yielding is highlighted in bold. (b) Micromechanical FE model in the initial configuration to an applied strain of 3%. Matrix yielding is shown in red.

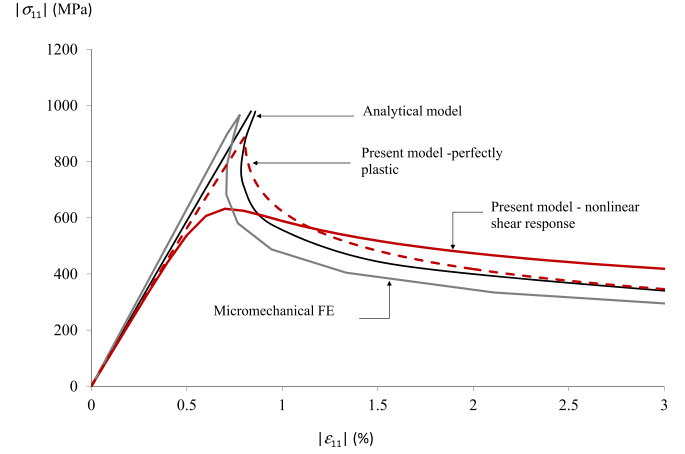


Fig. 6. Longitudinal compressive responses for the present model and the analytical and micromechanical FE models.

with a 3.5° initial misalignment and a perfectly plastic response in longitudinal shear. For the present model, the response with the actual nonlinear shear response is also given for comparison.

The three models assuming perfect plasticity agree fairly well with only moderate differences in the peak and crush stress values. These differences can be explained by the different assumptions taken in the three models. It can however be noted that consideration of a nonlinear shear response has an effect on the shape of the response as well as on the peak stress and crush stresses.

A further comparison is proposed between the state of damage in the kink-band between the different models. However, this cannot be done directly as the present model is based on continuum damage mechanics and the two others on perfect plasticity. It is proposed to compare the single damage variable, d , associated with matrix failure, of the present model with the length of the yield band, L_{yield} , divided by the final kink-band width, w , for the two other models. These two quantities are mathematically different but both represent the extent of nonlinearity in the matrix at a given strain, providing a qualitative comparison of the models. The final kink-band width is measured to 0.4 mm when the axial compressive stress in the fibres reaches 3200 MPa [20]. The comparison is shown in Fig. 7, the initiation of damage and trend of the growth are in good agreement. The damage parameter d of the present model appears to be slightly larger than L_{yield}/w in the other models.

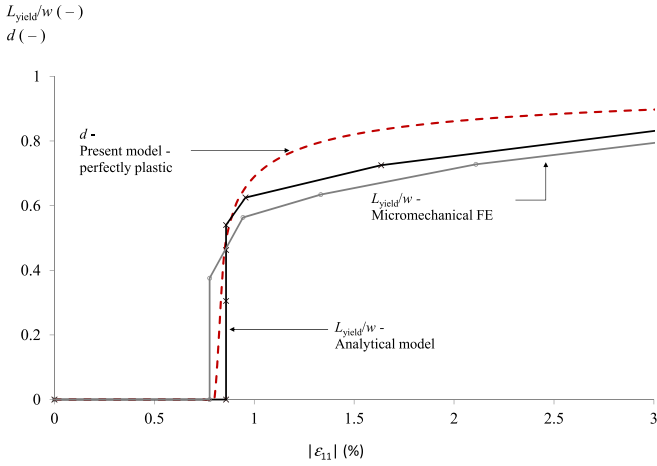


Fig. 7. Comparison of damage evolution in the present model with the yield zones in the analytical and micromechanical FE models.

4.2. Validation/comparison with experiments

It is hardly possible to validate the predicted kinking stress-strain relation by uniform axial loading, as fibre kinking is a local phenomenon, where the strain energy released by the surrounding material and test rig normally is sufficient to cause a sudden and catastrophic failure. Controlled failure is only possible in test specimens with high local stresses, e.g. at crack tips. A method to determine the cohesive law for fibre kinking was presented in Ref. [22], who used a waisted compact compression test specimen. The specimen manufacture is, however, complex and the evaluation currently relies on a number of simplifying assumptions.

The stress-strain relation predicted by the current model can, however, be partially validated by considering two particular test cases. In the first case, the peak stress and corresponding strain during uniform axial loading according to ASTM D 3410, as reported in Ref. [18], is considered. The corresponding stresses and strains at failure have been indicated by crosses in Fig. 8, and it is evident that the results are in good agreement with the model predictions for typical misalignment angles of 3° – 4° . The scatter in results reflects the strong influence of initial fibre misalignment angles.

The relatively large misalignment angle reflects the undulation in the current uni-weave NCF material. It should also be recognised

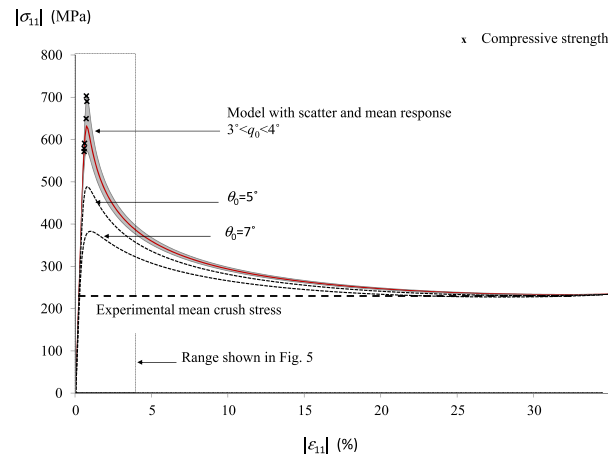


Fig. 8. Evolution of kinking stress vs. experimental results: Strength and mean crushing stress.

that the typical fibre misalignment in a 3D configuration is larger than what is observed in 2D micrographs, as it also is composed of out-of-plane components. Thus, for a transversely isotropic ply, superposition of components in the 2- and 3-directions implies $\theta_{i3D} \approx \sqrt{2}\theta_{i2D}$. Furthermore, the misalignment angle in the model also reflects other geometrical imperfections in fibre cross-section, initial fibre kinks, porosities etc.

In the second case, the axial crushing of unidirectional specimens with a triangular trigger is considered, as reported by Bru et al. [21]. The dashed line in Fig. 8 is located at 232 MPa and represents the mean crushing stress value of the four experiments, illustrated in Fig. 9.

Compressive failure in specimens with a trigger is initiated at a very early stage and the measured stress corresponds to the asymptotic stress for large compressive strains. The initial values of stress in Fig. 9 are not reliable due to the uncertainty of the initial trigger geometry. By using geometrical relations it was possible to verify that the average stress remained constant during crushing of the triangular trigger and during subsequent crushing of the region with constant cross section. The measured average crush stress has been indicated by a horizontal line in Fig. 8, and it is evident that it is in good agreement with the predicted stress for large compressive strains.

5. Discussion

The constitutive model presented here brings together a 3D formulation and a physically based description of the material in the kink-band, accounting for friction on the microcracks of the damaged material. It makes it possible to link with a single damage variable the transverse response, the longitudinal shear response and the longitudinal compressive response of the composite. The damage variable is associated with matrix failure and implies that fibre kinking is treated as a matrix failure mode. Besides simplifying the complexity of the model, such a formulation also simplifies the identification of the material parameters as the evolution of a single damage variable is required. The need to measure translaminar compressive toughness during fibre kinking is therefore removed. This is a significant improvement as these values are typically hard to measure and values ranging from 25 kJ/m^2 [22] to 79.9 kJ/m^2 [23] have been reported for similar carbon epoxy systems. Instead, the evolution laws for the two dissipating mechanisms, damage growth and friction, can be obtained from shear tests. Such tests are standardised for in-plane shear testing and are under investigation for out-of-plane shear testing.

The model developed in Ref. [15] for the longitudinal shear and

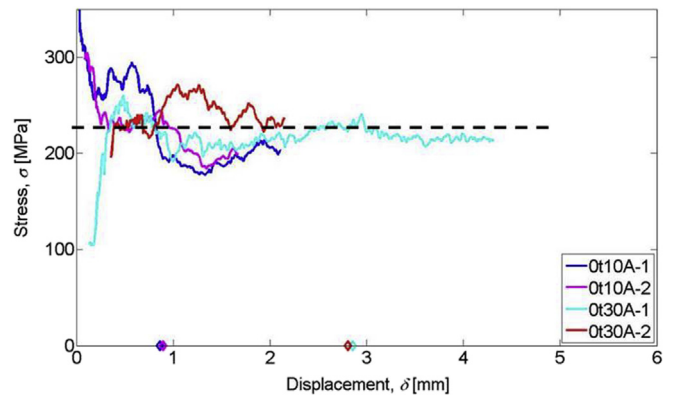


Fig. 9. Crushing response of longitudinal specimens with 10° and 30° trigger angles [21].

transverse responses provides an improvement to the model developed by Fleck et al. [8]. In particular the shear response shown in Fig. 4 provides a good representation of the nonlinear behaviour and of the hysteresis. It is however noted that viscoelastic effects are currently not included, which results in some discrepancies in the hysteresis cycles at large strains. It is also believed that not including viscoelasticity results in a faster growth rate for the damage variable and an increased effect of the friction.

The model presented here compares well with analytical and micromechanical FE models previously developed. Some discrepancies related to different assumptions by the different models are however shown in Figs. 6 and 7. In particular, the present model is a 3D model formulated at the ply level while the two other models are 2D models based on micromechanics.

The model is able to predict the longitudinal crush measured experimentally with input parameters that can be readily obtained from standard tests. This is of course important for future use in crush and crash applications. The model also gives an insight on the effect the initial fibre misalignment. It is interesting to see that while the initial fibre misalignment drastically reduces the strength it has an almost negligible effect on the crush stress. This can be explained by the fact that for large compressive strains, the kinked fibres have rotated to angles larger than 30° and the effect of a few degrees initially becomes, in relation to those large angles, less important.

The effect of the kink-band angle β has been discussed in the literature and by comparing the responses from the micro-mechanical FE analysis, which has a non-zero β angle, to the analytical and present models, which have $\beta = 0^\circ$, it can be inferred that it does not appear to play a significant role.

In the present study, matrix damage induced by longitudinal shear and transverse stresses is calculated and solved before solving for the longitudinal equilibrium. On one hand, this approach makes it possible to capture other types of matrix damage such as splitting, but on the other hand, it implies that the longitudinal response does not affect the transverse response. This is a reasonable assumption if loads are applied simultaneously but could lead to error for path dependent problems. Therefore, for a general 3D stress state, a convergence criterion between the damage variable calculated for matrix damage only and for the one calculated during kinking should be achieved, as shown in Fig. 3.

6. Conclusions

A physically based constitutive law to predict kink-band formation and growth has been proposed. 3D kinking theory is used together with a physically based constitutive law of the material in the kink-band. The full collapse response can be predicted and a crush stress can be extracted. The validation against experiments shows a very good correlation for the strength and failure strain values as well as the stress evolution for very large strains, i.e. crush stress.

The model is compared with an analytical model and a micro-mechanical finite element analysis. Despite the different assumptions of the models, a good agreement is found for the predicted responses but also the evolution of damage.

The proposed model eliminates the need for difficult and time

consuming experiments, i.e. the determination of the fibre kinking fracture toughness, which is usually required to model kink-band growth.

Taking advantage of the 3D formulation, the model will be implemented in an FE code for further validation at larger scale. Validation for multiaxial load cases will also be performed. Future work will address the extension to orthotropic materials which are more fully representative for textile reinforced composites.

References

- [1] S.T. Pinho, L. Iannucci, P. Robinson, Physically based failure models and criteria for laminated fibre-reinforced composites with emphasis on fibre kinking. Part II: FE implementation, *Compos. Part A* 37 (5) (2006) 766–777.
- [2] C.S. Yerramalli, A.M. Waas, A non-dimensional number to classify composite compressive failure, *J. Appl. Mech.* 71 (2004) 402–408.
- [3] R. Gutkin, S.T. Pinho, P. Robinson, P.T. Curtis, On the transition from shear-driven fibre compressive failure to fibre kinking in notched CFRP laminates under longitudinal compression, *Compos. Sci. Technol.* 70 (2010) 1223–1231.
- [4] P. Prabhakar, A.M. Waas, Interaction between kinking and splitting in the compressive failure of unidirectional fiber reinforced composites, *Compos. Struct.* 98 (2013) 85–92.
- [5] B.W. Rosen, Mechanics of composite strengthening, in: *Fiber Composite Materials*, Ch. 3, American Society for Metals, Metals Park, OH, 1965, pp. 37–75.
- [6] A.S. Argon, Fracture of composites, in: *Treatise on Materials Science and Technology*, vol. 1, Academic Press, New York, NY, 1972, pp. 79–114.
- [7] B. Budiansky, *Micromech. Comput. Struct.* 16 (1–4) (1983) 3–12.
- [8] N.A. Fleck, Compressive failure of fibre composites, *Adv. Appl. Mech.* 33 (1997) 43–119. Academic Press.
- [9] S. Basu, A.M. Waas, D.R. Ambur, A macroscopic numerical model for kink banding instabilities in fiber composites, *J. Mech. Mater. Struct.* 1 (6) (2006) 979–1000.
- [10] N.A. Fleck, L. Deng, B. Budiansky, Prediction of kink width in compressed fiber composites, *J. Appl. Mech.* 62 (2) (1995) 329–337.
- [11] S. Pimenta, R. Gutkin, S.T. Pinho, P. Robinson, A micromechanical model for kink-band formation: Part II—Analytical modelling, *Compos. Sci. Technol.* 69 (7–8) (2009) 956–964.
- [12] P. Davidson, A.M. Waas, Mechanics of kinking in fiber-reinforced composites under compressive loading, *Math. Mech. Solids* 21 (6) (2014) 667–684.
- [13] S. Basu, A.M. Waas, D.R. Ambur, Compressive failure of fiber composites under multi-axial loading, *J. Mech. Phys. Solids* 54 (3) (2006) 611–634.
- [14] Pinho ST, Dávila CG, Camanho PP, Iannucci L, Robinson P. Failure Models and Criteria for FRP under In-plane or Three-dimensional Stress States Including Shear Non-linearity. NASA/TM-2005–213530.
- [15] R. Gutkin, S.T. Pinho, Combining damage and friction to model compressive damage growth in fibre-reinforced composites, *J. Compos. Mater.* 49 (2015) 2483–2495.
- [16] K. Park, G.H. Paulino, J.R. Roesler, A unified potential-based cohesive model of mixed-mode fracture, *J. Mech. Phys. Solids* 57 (2009) 891–908.
- [17] M.J.D. Powell, An efficient method for finding the minimum of a function of several variables without calculating derivatives, *Comput. J.* 7 (2) (1964) 155–162.
- [18] T. Bru, P. Hellström, R. Gutkin, D. Ramantani, G. Peterson, Characterisation of the mechanical properties of a uni-weave carbon fibre/epoxy non-crimp fabric composite, *Data Brief* 6 (2016) 680–689.
- [19] S. Pimenta, R. Gutkin, S.T. Pinho, P. Robinson, A micromechanical model for kink-band formation: Part I—Experimental and numerical modelling, *Compos. Sci. Technol.* 69 (7–8) (2009) 948–955.
- [20] R. Gutkin, S.T. Pinho, P. Robinson, P.T. Curtis, Micro-mechanical modelling of shear-driven fibre compressive failure and of fibre kinking for failure envelope generation in CFRP laminates, *Compos. Sci. Technol.* 70 (8) (2010) 1214–1222.
- [21] T. Bru, P. Waldenström, R. Gutkin, R. Olsson, G. Vyas, Development of a novel flat specimen for measuring the crush stress of unidirectional laminates, *Compos. Part A Appl. Sci. Manuf.* (2016). Submitted.
- [22] D. Svensson, K.S. Alfredsson, U. Stigh, N.E. Jansson, Measurement of cohesive law for kink-band formation in unidirectional composite, *Eng. Fract. Mech.* 151 (2016) 1–10.
- [23] S.T. Pinho, P. Robinson, L. Iannucci, Fracture toughness of the tensile and compressive fibre failure modes in laminated composites, *Compos. Sci. Technol.* 66 (13) (2006) 2069–2079.